ROS-derived lipid peroxidation is prevented in barley leaves during senescence

Ginga Shimakawa, Anja Krieger-Liszkay, Thomas Roach

▶ **To cite this version:**

Ginga Shimakawa, Anja Krieger-Liszkay, Thomas Roach. ROS-derived lipid peroxidation is prevented in barley leaves during senescence. Physiologia Plantarum, 2022, 174, pp.e13769. 10.1111/ppl.13769 . hal-03853488

HAL Id: hal-03853488
https://hal.science/hal-03853488

Submitted on 15 Nov 2022

HAL is a multi-disciplinary open access archive for the deposit and dissemination of scientific research documents, whether they are published or not. The documents may come from teaching and research institutions in France or abroad, or from public or private research centers.

L'archive ouverte pluridisciplinaire **HAL**, est destinée au dépôt et à la diffusion de documents scientifiques de niveau recherche, publiés ou non, émanant des établissements d'enseignement et de recherche français ou étrangers, des laboratoires publics ou privés.

Distributed under a Creative Commons Attribution 4.0 International License

ROS-derived lipid peroxidation is prevented in barley leaves during senescence

Ginga Shimakawa[1,2], Anja Krieger-Liszkay[2] Thomas Roach[3,*]

[1]Department of Bioscience, School of Biological and Environmental Sciences, Kwansei-Gakuin University, 2-1 Gakuen, Sanda, Hyogo 669-1337, Japan

[2]Université Paris-Saclay, Institute for Integrative Biology of the Cell (I2BC), CEA, CNRS, 91198 Gif-sur-Yvette cedex, France

[3]University of Innsbruck, Department of Botany, Innsbruck, 6020, Austria

*corresponding author thomas.roach@uibk.ac.at

Abstract

Senescence in plants enables resource recycling from senescent leaves to sink organs. Under stress, increased production of reactive oxygen species (ROS) and associated signalling activates senescence. However, senescence is not always associated with stress since it has a prominent role in plant development, in which the role for ROS signalling is less clear. To address this, we investigated lipid metabolism and patterns of lipid peroxidation related to signalling during sequential senescence in first-emerging barley leaves grown under natural light conditions. Leaf fatty acid compositions were dominated by linolenic acid (75 % of total), the major poly-unsaturated fatty acid (PUFA) in galactolipids of thylakoid membranes, known to be highly sensitive to peroxidation. Lipid catabolism during senescence, including increased lipoxygenase activity, led to decreased levels of PUFA and increased level of short-chain saturated fatty acids. When normalized to leaf area, only concentrations of hexanal, a product from the 13-lipoxygenase pathway, increased early upon senescence, whereas reactive electrophile species (RES) from ROS-associated lipid peroxidation, such as 4-hydroxynonenal, 4-hydroxyhexenal and acrolein, as well as β-cyclocitral derived from oxidation of β-carotene, decreased. However, relative to total chlorophyll, amounts of most RES increased at late-senescence stages, alongside increased levels of α-tocopherol, zeaxanthin and non-photochemical quenching, an energy dissipative pathway that prevents ROS production. Overall, our results indicate that lipid peroxidation derived from enzymatic oxidation occurs early during senescence in first barley leaves, while ROS-derived lipid peroxidation associates weaker with senescence.

Introduction

Leaf senescence is an important nutrient-recycling process in higher plants, and seen as the last stage of leaf development (Lim et al., 2007). It is endogenously regulated, but can be induced by exogenous parameters, such as stress. Endogenous regulation occurs via phytohormone and sugar levels, protein phosphorylation, and potentially reactive oxygen species (ROS), which each have varying influence depending upon age of leaf and developmental state of the plant. During senescence, cellular constituents are degraded in a coordinated manor to enable nutrient availability for sink organs, such as seeds or new leaves, depending upon the developmental state of the plant and its growth strategy (i.e. monocarpic or perennial). Developmental senescence can be divided into two stages; first 'sequential senescence' whereby resources are reallocated from old to young leaves, and second, 'reproductive senescence' of monocarpic species (e.g. annuals) in which resources are made available for seed production (Thomas, 2013). Leaves that house photosynthetic machinery are resources for growth, such as N-rich light harvesting complexes (LHC), also called 'antenna', and the highly abundant RuBisCO enzyme.

ROS are clear candidates of chloroplast-derived signals that may play a role in triggering senescence (Krieger-Liszkay et al., 2019). Regarding developmental senescence, hydrogen peroxide (H_2O_2) has emerged as such a signal in mature monocarpic annual plants before flowering (Bieker et al., 2012; Zentgraf et al., 2022). In support of this hypothesis, several senescence-associated transcription factors are responsive to H_2O_2 (Balazadeh et al., 2011; Garapati et al., 2015; Zentgraf and Doll, 2019). Furthermore, ROS-mediated oxidative modifications (e.g. protein carbonyls, aldehydes/alkenals from lipid peroxidation etc.) accumulate in senescing leaf chloroplasts during reproductive senescence, and there are clear overlaps between photo-oxidative responses and senescence, although most of these reports are from plants under stress (Pintó-Marijuan and Munné-Bosch, 2014). Of note, H_2O_2 is produced from various peroxisome-located oxidases in catabolism, as well as from dismutation of superoxide ($O_2^{\bullet-}$) produced by electron leakage from electron transport chains of respiration and photosynthesis (Halliwell, 2006). The ROS singlet oxygen ($^1O_2$) is predominantly produced by excited chlorophyll in its triplet state in the photosystem II (PSII) reaction centre, or LHC in the PSII grana core (Dogra and Kim, 2020; Krieger-Liszkay, 2005). $^1O_2$ is highly oxidizing, and has a prominent role in oxidative modifications of thylakoid membranes, leading to lipid peroxidation (Triantaphylidès et al., 2008; Biswas & Mano, 2021), and release of reactive electrophile species (RES) that can activate a large proportion of the $^1O_2$ signalling pathway (Mano et al., 2019; Roach et al., 2018). Furthermore, oxidation of the β-carotene located in the PSII reaction centre releases the RES β-cyclocitral that can be involved in $^1O_2$-mediated signalling of *Arabidopsis thaliana* (Ramel et al., 2013). Lipid oxidation via the lipoxygenases (LOX) pathway also leads to production of six-carbon aldehydes, such as hexanal (hexaldehyde) and oxylipins phytohormones

called jasmonates. Besides functioning in abiotic and biotic stress responses, jasmonates may play a role in senescence signalling (Seltmann et al., 2010), particularly in monocot plants (Bachmann et al., 2002), as well as in the breakdown of the plastid envelope (Springer et al., 2016). However, if aldehyde/RES initiate signalling pathways that activate sequential leaf senescence in non-stressed leaves is less clear.

In this study, we used two barley cultivars, cv. Lomerit and cv. Carina, to investigate patterns of lipid peroxidation, as markers of ROS and LOX activity, during senescence of first leaves grown in a glasshouse under natural light regimes. In monocarpic annual crops, such as barley, sequential senescence occurs early in plant development to facilitate growth of the shoot and new leaves (Distelfeld et al., 2014; Gregersen et al., 2008). Under outdoor conditions, the first leaf of barley cv. Lomerit and cv. Carina starts to senesce two weeks after sowing seeds when grown in small pots (Shimakawa et al., 2020). In first barley leaves of these cultivars, no differences in production rates of $O_2^{\bullet-}/H_2O_2$, between early (17 days after sowing) and later (31 days after sowing) stages of senescence were found, while rates of $^1O_2$ production increased in cv. Lomerit, but not in cv. Carina at the later stage (Shimakawa et al., 2020). Therefore, the question arises whether ROS/RES play a role in activating sequential senescence in non-stressed plants. Considering profiles of ROS production in leaves of these cultivars during senescence (Krieger-Liszkay et al., 2015; Shimakawa et al., 2020), we hypothesised that mechanisms are activated that protect against ROS production in the chloroplast, or prevent ROS-mediated lipid peroxidation from propagating (i.e. antioxidants).

Material and Methods

Plant material

The winter barley cultivar Lomerit (*Hordeum vulgare* L., cv. Lomerit) and the spring cultivar Carina (*Hordeum vulgare* L., cv. Carina) were grown in pots (5-9 plants per 6 × 6 cm pot) in commercial germination soil (Fruhstorfer Erde, Hawita), in non-controlled conditions in summer (from June to July) in a green-house at the Institute of Botany, University of Innsbruck, Austria. Air temperature and light intensity immediately next to the plants (Fig. S1) were measured with an Easy EL-USB-1-LCD data logger (Lascar) and SE-SQ520 sensor (Apogee Electronics, Santa Monica, US), respectively. The first emerging unfolded leaf from the coleoptile, hereafter 'first leaf', of cv. Lomerit and cv. Carina were used for all experiments before and after onset of natural senescence (Fig. S2).

Chlorophyll fluorescence and near infrared absorbance analyses

Maximum quantum efficiency of PSII photochemistry (F_v/F_m) and total photo-oxidizable P700 (P_m) were non-invasively determined on attached leaves with a Dual-PAM-100 (Walz, Effeltrich,

Germany). For the chlorophyll fluorescence measurements, the first barley leaves were dark adapted for 15 min. A pulse-amplitude modulated red measuring light (620 nm, 0.1 µmol photons m^{-2} s^{-1}) was used to obtain F_o (minimum fluorescence from dark-adapted leaves). For the determination of F_m (maximum fluorescence from dark-adapted leaves), a short-saturation flash (8,000 µmol photons m^{-2} s^{-1}, 300 ms) was provided by the LED array. F_v/F_m was calculated as $(F_m - F_o)/F_m$ (Baker, 2008). For P700 measurements, the leaves were taken from the light. The transmittance of oxidized P700 ($P700^+$) was measured by pulse-amplitude modulated near-infrared measuring lights (830 and 870 nm) (Klughammer and Schreiber, 1994). The light guide was restricted to minimum leaf width using black insulation tape (in total 0.45 cm^2). The full oxidation level of P700 was determined by the 300-ms short-saturation flash after 10 s far-red light illumination (730 nm), and the full reduction level of P700 was defined in the dark, resulting in the P_m values.

Non-photochemical quenching (NPQ) of barley first leaves was measured with an Imaging-PAM (Walz). Pulse-modulated excitation, actinic illumination, and saturation flashes were achieved with a blue LED lamp with a peak emission of 450 nm. The actinic light intensity was set at 1250 µmol photons m^{-2} s^{-1}, and NPQ was calculated as $(F_m\text{-}F_m')/F_m'$, with F_m' the maximum fluorescence emission from light-adapted leaves. F_m and F_m' were determined using saturating flashes (8,000 µmol photons m^{-2} s^{-1}).

Pigments, aldehydes and RES quantification

Plants were sampled in the afternoon and taken from direct sunlight (intensity 1000-1100 µmol photons m^{-2} s^{-1}). Measurements of P_m were made of leaf segments, without dark adaption. After cutting the leaf segment from the first leaf, the dimensions (width, length) were rapidly measured before freezing in liquid nitrogen in a 2 mL reaction tube with two 3 mm glass beads. The process was repeated for each leaf segment one by one. Extraction was made in 1.0 mL acetonitrile by shaking at 30 Hz for 2 mins. After centrifugation for 10 min at 29,000 *g* and 4 °C, the supernatant was split. An aliquot of sample (15 µl injection volume) was used for simultaneous measurements of pigments, measured via a diode array detector (absorption at 440 nm), and tocopherols, measured with fluorescence detector (Ex: 295 nm; Em: 325 nm), using an Agilent 1100 HPLC (Roach et al., 2017). Aldehydes and RES in 400 µl of the supernatant were derivitised with 2,4-dinitrophenylhydrazine, along with 0.5 µM 2-ethylhexanal (as internal standard) and 0.005% (w/v) of butylated hydroxytoluene, using LC-MS/MS (Roach et al., 2017).

Lipids and lipoxygenase activity

Plants were sampled as for other biochemical analyses, except from freeze-dried leaf segments. Total fatty acids (e.g. membranes, storage lipids, free fatty acids) of cv. Carina were extracted in 1.0 mL of methanol:toluene:sulfuric acid 40:12:1 (v:v:v), containing 0.01% (w:v) butylated hydroxytoluene, and

heptadecanoic acid (C17:0), as internal standard. After derivatisation to fatty acid methyl esters (FAMEs), samples were analysis by gas chromatography coupled with mass spectrometry (GC-MS), as previously described (Schausberger et al., 2019), and normalised to dry weight (DW). Relative changes were based on peak area for selected fragments of each fatty acid, whereas relative fatty acid composition after treatments were evaluated by peak areas of total ion current (TIC) chromatograms for each fatty acid. For thin-layer chromatography of membrane lipids, lipids were extracted in chloroform/methanol (1:2, v/v), with extraction volume adjusted according to sample DW, before separation and detection on silica gel 60 plates with concentration zones (Merck Millipore, US) impregnated with ammonium sulphate, according to Wewer et al., (2013). Bands were assigned with pure standards purchased from Avanti Polar Lipids (Alabaster, US), and qunatified using densiosemtry.

For measuring lipoxygenase activity, ground leaf segments of cv. Carina were extracted in 500 µL of 50 mM TRIS buffer, pH 7.0, centrifuged for 10 min at 29,000 *g* and 4 °C, and 50 µL of the supernatant was added to 150 µL 50 mM TRIS buffer, pH 7.0, containing 2 µL of 5 mM linoleic acid dissolved in dimethyl sulfoxide in a UV-transparent 96-well plate (Brand, Germany). Lipid peroxide formation was measured at 234 nm every 15 s between 1-5 min at 30 °C, with two technical replicates per biological replicate, using the 0.1 m^2/mol extinction coefficient of 27,000 and a 0.5cm light path-length. Activity was normalised to protein amount, measured in two technical replicates each of 5 µL extract, using the Bradford Assay (BioRad, Germany).

Spin-trapping electron paramagnetic resonance measurements

Electron paramagnetic resonance (EPR) spin-trapping assays for determining H_2O_2 were carried out using the spin trap 4-pyridyl-1-oxide-N-tert-butylnitrone (4-POBN) (Sigma-Aldrich, US). Leaves were vacuum-infiltrated with a buffer (25 mM HEPES, pH 7.5, 5 mM $MgCl_2$, 0.3 M sorbitol) containing the spin trap reagents (50 mM 4-POBN, 4% ethanol, 50 µM Fe-EDTA). Infiltrated leaves were placed into the buffer containing the spin trap reagents and illuminated for 1 h with white light (200 µmol photons m^{-2} s^{-1}). At the end of the illumination time, the leaves were removed and the EPR signal of the solution was monitored. EPR spectra were recorded at room temperature in a standard quartz flat cell using an ESP-300 X-band (9.73 GHz) spectrometer (Bruker, US). The following parameters were used: microwave frequency 9.73 GHz, modulation frequency 100 kHz, modulation amplitude: 1 G, microwave power: 6.3 mW, receiver gain: 2 x 104, time constant: 40.96 ms; number of scans: 4. The EPR signal sizes were normalized by the total chlorophyll contents of each sample.

Statistics

Six random plants of each cultivar were selected at each of the six time points for measurements. For regression analysis of P_m with biochemical parameters, log-normal fitting was conducted in OriginPro

2017G for both cultivars collectively, or with photosynthetic parameters for each cultivar separately. For calculating *P* values over time for both cultivars, or between cultivars over all time points, a univariate general linear model was used in IBM SPSS Statistics 25.

Results

Leaf senescence and photosynthesis

Barely seeds of two cultivars, Carina and Lomerit, were sown on six occasions during two time courses, so that each of the two time courses ended with first leaves of differing degree of senescence (Fig. S1). This was chosen so that leaves of different age had experienced the same environmental conditions before measurements. First leaves were measured 13, 20 and 27 days (time course 1), or 18, 25 and 32 days (time course 2), since seeds had been sown (Fig. S1A). Light intensity in the naturally lit glasshouse used for growing plants reached 1300 µmol photons m^{-2} s^{-1} on cloudless days, and up to 250 µmol photons m^{-2} s^{-1} when overcast (Fig. S1A). Due to partial shading from trees above, plants were subjected to fluctuating, rather than slowly changing, light intensities (Fig. S1B). Average temperature during the entire growing period was 24.3 °C, with typically a 10-15 °C difference between maximum day and minimum night temperatures (Fig. S1A). Of note, plants from the first course had experienced warmer maximum temperatures in the week before measurement than those from the second time course (Fig. S1).

As senescence indicators, we measured maximum quantum efficiency of PSII (F_v/F_m), maximum photo-oxidizable P700 levels (P_m), and total chlorophyll content. In accordance with a previous study of the same cultivars (Shimakawa et al., 2020), the magnitude in decline of P_m during senescence was greater than the loss of F_v/F_m (Fig. 1A), and P_m declined earlier than F_v/F_m (Fig. 1B). Thus, we chose P_m as a reference to the degree of leaf senescence throughout this study. This non-destructive measurement was made immediately before biochemical measurements, enabling correlation of P_m with other parameters for 72 individual first leaves, with six replicate leaves for each cultivar for each of the six different ages of first leaves. Levels of total chlorophyll linearly correlate with P_m, with Pearson R values of 0.67 and 0.78 for cv. Lomerit and cv. Carina, respectively, (Fig. 1C). In all three senescent indicators, no distinguishable difference between cultivars is observable (Fig. 1).

Regarding photosynthesis-related carotenoids, levels of lutein and neoxanthin remained similar relative to total chlorophyll, while antheraxanthin and zeaxanthin levels increased and violaxanthin decreased (Fig. S3; Tab. S1), significantly shifting the xanthophyll de-epoxidation ratio at later stages of senescence (Fig. 2A; Tab. S1), also when chlorophyll content was used as a senescence marker (Fig. S4). Activation of the xanthophyll cycle agrees with the significant increase

in NPQ observed in late-senescent leaves (Fig. 2B), i.e. when P_m values had decreased by ca. 60% (Fig. 1A). During senescence, levels of β-carotene found in the reaction centre of PSII and the core complexes of PSI decreased relative to total chlorophyll (Fig. S3; Tab. S1), showing overall that changes in pigments are not uniform and that reaction centres are likely broken down before antenna. In support of this, the chlorophyll *a*:*b* ratio significantly decreased as senescence progressed (Fig. S4; Tab. S1).

Reactive electrophile species, hexaldehyde and lipoxygenase activity

When normalised to total chlorophyll, concentrations of hexaldehyde and RES increased during senescence, with the exception of 2-hexenal (Fig. 3A). Correlation of absolute concentrations with P_m generally revealed log-normal relationships for all species quantified (Fig. S5). Hexaldehyde was the only specie that significantly increased consistently after 13 days since sowing seeds, and has the strongest log-normal R^2 value with P_m of 0.61 (Fig. S5). This is partly due to low hexaldehyde concentrations (<0.5 μmol mol^{-1} total chlorophyll) only found in leaves with a P_m >0.45 and high concentrations (>3.0 μmol mol^{-1} total chlorophyll) only found in leaves with a P_m <0.3 (Fig. S4). The RES acrolein was at similar concentration to hexaldehyde (up to 4.5-5.5 μmol mol^{-1} total chlorophyll; Fig. S5), but increased less during senescence (Fig. 3A). Overall, relationships of RES with P_m were relatively weak. For example, malondialdehyde, often the most abundant specie (up to 14 μmol mol^{-1} total chlorophyll), had a log-normal R^2 value with P_m of 0.15 when considering both cultivars together. In pre or early-senescing leaves (P_m >0.5), concentrations of β-cyclocitral were 0.2-0.3 μmol mol^{-1} total chlorophyll, and the ratio of β-cyclocitral:β-carotene are ca. $1:2x10^6$, while in late-senescing leaves (P_m <0.2) β-cyclocitral concentrations were up to 0.9 μmol mol^{-1} total chlorophyll, and have a typical ratio to β-carotene of $1:1x10^5$. However, some late-senescing leaves possessed equal β-cyclocitral concentrations as pre-senescent leaves, leading to a low log-normal R^2 value with P_m of 0.38 (Fig. S5). Similar to fomaldehyde (Fig. S4), other short-chain aldehydes, including acetylaldehyde, propionaldehyde, butyraldehyde, benzylaldehyde and valeraldehyde only significantly increased, relative to chlorophyll, at late stages of senescence (data not shown).

When normalised to leaf area, hexaldehyde was the only species consistently found at higher concentrations at 18-32 days, compared to 13 days, after sowing seeds (Fig. 3B). Lipoxygenase activity, a potential source of hexaldehyde, was barely detectable in leaves before senescence and only increased when P_m decreased to values <0.5, after which activity increased as senescence progressed (Fig. 3C). On a leaf area basis, the RES acrolein, 4-hydoxynonenal (HNE), 4-hydroxyhexenal (HHE), 2-pentenal and 2-hexenal declined as senescence progressed (Fig. 3B), concomitantly with the decrease in chlorophyll content. No senescence-related increase in light-induced $O_2^{\bullet-}/H_2O_2$ production, as measured with EPR spin-trapping, in leaves of either genotype was observed during the observation period (Fig. S6).

Together, normalisation to chlorophyll and leaf area indicate that RES are generated within the chloroplast, that the production is probably linked to $^1O_2$ production rather than $O_2^{\bullet-}/H_2O_2$ production, but that these RES do not accumulate in leaves early in senescence.

α-tocopherol and lipid composition

Concentrations of α-tocopherol, relative to total chlorophyll, consistently increased during senescence (Fig. 4A), as shown by log-normal R^2 values with P_m of 0.75 and 0.81 for cv. Lomerit and cv. Carina, respectively. γ-tocopherol changed similarly, but was at lower concentrations than α-tocopherol, with half the samples below detection limit (Fig. 4A). A similar trend was observed when using chlorophyll content as a senescence marker (Fig. S4). When normalised to leaf area, the same trend is apparent of increased concentrations as senescence progressed (Fig. 4B), although weaker R^2 values 0.54 and 0.13, respectively. In both cases, concentrations in cv. Lomerit increased more than cv. Carina, and the relationship with chlorophyll was closer than with leaf area (Fig. 4).

Lipid composition during senescence was monitored by changes in amounts of each fatty acid and membrane groups in cv. Carina. After 18 days since sowing seeds, linolenic acid (C18:3) constituted 75 % of the total fatty acid pool in first leaves, followed by palmitic acid (C16:0; 16 %), linoleic acid (C18:2; 4 %), stearic acid (C18:0; 2 %) and palmitoleic acid (C16:1; 1 %), with unsaturated fatty acids composing 80 % of total fatty acids (Fig. 5A). After 25 days since sowing (mid senescence, P_m had decreased by 40-45 %) levels of unsaturated fatty acids decreased, while levels of saturated fatty acids increased, especially short-chain (C10:0-C15:0) species, with the exception of C16:0 that decreased (Fig. 5B). This trend tended to continue to 32 days (late senescence, P_m decreased by ca. 65 %), but to a lesser extent (Fig. 5B), so that unsaturated fatty acids composed 72 % of total fatty acids. Concerning membrane groups, galactolipids (MGDG, DGDG and SQDG) of the thylakoid membrane were most abundant in first leaves 18 days since onset of germination (Fig. 5C). They decreased to a greater extent than the detected phospholipids (PG, PC) (Fig. 5D). This clearly demonstrates that thylakoid membranes are degraded during senescence.

Principal component integration of photosynthetic and lipid-associated parameters

Principal component (PC) analysis of all aforementioned data measured in both cultivars, and using relative changes of aldehyde/RES concentrations normalised to chlorophyll, separated samples due to age on PC1, which accounted for 40.5% of total variance (Fig. 6). Of note, the grouping amongst leaves of the same age on PC1 weakened as leaves aged, as did the overlap between groups of leaves in each age category, highlighting increasing variability between leaves as senescence progressed. The loading plot showed that decreases in established senescent markers (i.e. F_v/F_m, P_m, total chlorophyll) separated leaves along PC1 in a different direction to the increase in tocopherols and aldehydes and RES, with the exception of RES trans-2-penetenal and HHE since these two species showed only a

weaker relationship with leaf age. Variation between leaves in every age category separated on PC2, which accounted for 18.7% of total variance, and was influenced by differences in carotenoids between leaves of the same age (Fig. 6).

Discussion

The production of ROS is unavoidable from excited chlorophyll and during photosynthetic electron transport, which can lead to lipid peroxidation of PUFA-rich thylakoid membranes and the production of lipid hydroperoxides. Aldehydes and RES are subsequently released from spontaneous or ROS-dependent decomposition and hydroperoxide lipase activity (Farmer and Mueller, 2013; Griffiths et al., 2000). Various pathways exist for further breakdown, because accumulation of such species leads to cell toxicity (Farmer and Mueller, 2013; Mano, 2012; Roach et al., 2018). Although stress-induced senescence associates with lipid peroxidation, and studies with antioxidant knock-out mutants have shown that elevated RES levels can induce senescence (Nurbekova et al., 2021; Srivastava et al., 2017), it remains open if ROS-induced RES production plays a role in non-stress associated developmental senescence.

In the two barley varieties investigated here, several RES accumulated during senescence when RES was normalised to chlorophyll (Fig. 3A). These included acrolein, β-cyclocitral, 4- HHE and HNE that are known to be generated by ROS. Inactivation of the photosynthetic electron transport chain leads to excitation pressure in PSII and consequently an increase in ROS production. During senescence, photosynthetic electron transport decreased first at the level of PSI, as seen by the loss in P_m, followed by a loss in F_v/F_m, reflecting a loss in active PSII (Fig. 1), potentially leading to elevated ROS production. $^1O_2$ is a major source of lipid peroxidation in the chloroplast, but $^{\bullet}OH$ radicals derived from $O_2^{\bullet-}/H_2O_2$ are also able to oxidize lipids. In both, first and flag leaves, $^1O_2$ production increased only in cv. Lomerit during senescence when measured in isolated thylakoids (Krieger-Liszkay et al., 2015; Shimakawa et al., 2020). In the presence of α-linolenic acid, $^1O_2$ can lead to formation acrolein, which accumulates under stress in the chloroplast (Mano, 2012; Roach et al., 2020). The increase in acrolein was significant for cv. Lomerit, but not for cv. Carina at the latest stage of senescence (Fig. 3A), and a significant effect of cultivar was found over all time points (Tab. S1). Other non-enzymatic lipid peroxide products of α-linolenic acid include HHE and malondialdehyde, while HNE is produced from linoleic acid (Schneider et al., 2005), but no clear pattern connected these RES during senescence. In addition, β-cyclocitral, generated by $^1O_2$-induced oxidation of β-carotene, and potentially involved in $^1O_2$ signalling (Ramel et al., 2013), increased at late senescent stages relative to chlorophyll, but no clear difference between cv. Lomerit and cv. Carina was observed. During senescence, $O_2^{\bullet-}$ levels increased in thylakoids isolated from flag leaves of the two barley cultivars grown in the field (Krieger-Liszkay et al., 2015), but not in first leaves (Fig. S6; Shimakawa

et al., 2020). This difference may be caused by a higher antioxidant level in chloroplasts in first leaves than in flag leaves. A gradual increase in lipid peroxidation and a transient increase in $O_2^{\bullet-}/H_2O_2$ was observed during senescence in a study on second barley leaves, with highest levels of lipid peroxidation occurring at the late stages of senescence (Jajić et al., 2015).

In contrast to the increase in RES and aldehyde contents during senescence relative to total chlorophyll, hexaldehyde was the only species that consistently accumulated relative to leaf area (Fig. 3B). Previously, a chloroplast-located lipoxygenase, 13-LOX that binds to the chloroplast membrane of barley leaves, was identified to break down this plastid structure during senescence to release stromal constituents (Springer et al., 2016). 13-LOX catalyses stereospecific oxygenation of fatty acids forming 13-hydroperoxides, which are further broken down by 13-hydroperoxide lyase to release aldehydes. When linoleic acid is the substrate of 13-LOX, hexaldehyde is the product of the lyase, whereas with linolenic acid hexenal is produced (Montillet et al., 2004). Therefore, the accumulation of hexaldehyde and the decrease in linoleic acid support an involvement of 13-LOX-mediated degradation of the chloroplast membrane during senescence. In support of this, lipoxygenase activity increased as senescence progressed (Fig. 3C). The LOX pathway may also have a role in senescence via the synthesis of jasmonates (Hu et al., 2017; Seltmann et al., 2010), which in monocot plants (i.e. barley) further promote senescence (Bachmann et al., 2002).

As shown in Fig. 3 and Fig. S4, there is no clear difference in the concentrations of most RES between the two barley cultivars despite that cv. Lomerit produces more $^1O_2$ (Shimakawa et al., 2020). This suggests that the antioxidant system is capable of controlling RES levels in both cultivars. Zeaxanthin and α-tocopherol levels increased during senescence in both cultivars, but considerably more for cv. Lomerit (Fig. 4; Tab. S1). Since α-tocopherol can very efficiently scavenge $^1O_2$ (Krieger-Liszkay and Trebst, 2006), these results indicate first, that barley leaves were preventing ROS-mediated lipid peroxidation by elevating α-tocopherol concentrations, and second, why ROS associated RES levels were generally similar between cultivars. However, the increase of α-tocopherol may also reflect an increase of size and number of plastoglobuli, a phenomenon commonly observed during leaf senescence (van Wijk and Kessler, 2017). It should also be noted that RES are scavenged in leaves by enzymes, such as various aldo-keto reductase/dehydrogenases/oxidases and 2-alkenal reductase (Mano, 2012; Shimakawa et al., 2014). In *A. thaliana* leaves, elevating aldehyde dehydrogenase levels accelerated aldehyde breakdown and improved stress tolerance (Sunkar et al., 2003), while in leaves and siliques, aldehyde oxidases break down natural levels of RES under growth chamber conditions, preventing premature senescence (Nurbekova et al., 2021; Srivastava et al., 2017). Production of $^1O_2$ can also be prevented in the first place by thermal dissipation of excess light energy (i.e. NPQ) (Roach and Krieger-Liszkay, 2019). Therefore, the increase in NPQ during senescence (Fig. 2) may also have helped to prevent $^1O_2$-mediated lipid peroxidation. NPQ levels were

a bit lower in cv. Carina than in cv. Lomerit, and similar to the difference in VAZ de-epoxidation levels there was a significant effect of cultivar for antheraxanthin and zeaxanthin when considering all time points collectively (Tab. S1). According to the PCA, variation in xanthophyll composition was a cause for separation of leaves of the same age of both cultivars, indicating that each leaf had different exposure to light intensity at time of harvesting. Therefore, adjustments to NPQ involving antheraxanthin and zeaxanthin were likely compensating for short term changes in light exposure, helping prevent ROS production. An increase in NPQ accompanied by an increase in zeaxanthin and antheraxanthin during senescence has been observed previously in field-grown wheat leaves (Lu et al., 2001).

In summary, the first step of senescence in the greenhouse-grown barley cultivars was the decrease in chlorophyll contents and P_m values, followed later by a loss of F_v/F_m and increase in NPQ (Figs. 1,2). Lipoxygenase activity increased, and 13-LOX activity using linoleic acid as substrate was detected via accumulation of hexaldehyde. β-carotene seems to decrease linearly with PSI activity (Fig. S3), while α-tocopherol started to increase later in an exponential manner (Fig. 4). In *A. thaliana* upon light stress, first α-tocopherol is consumed and then, in a second stage, carotenoids (Kumar et al., 2020). However, in first barely leaves, our data support the hypothesis that $^1O_2$ reacts first with β-carotene in the reaction centres and, when this is largely consumed, α-tocopherol acts as scavenger. This shows that the importance of the antioxidants may differ depending on the physiological situation. Since β-carotene oxidation products have signalling roles, it would be tempting to suggest that they act as a trigger of the signalling pathway leading to controlled natural senescence. However, β-cyclocitral like other $^1O_2$-derived RES did not increase early during senescence, suggesting that such species likely do not trigger the onset of natural developmental senescence in barley although they may be involved in signalling events triggering later steps of senescence.

Availability of data: The data that support the findings of this study are available from the corresponding author upon reasonable request.

Author contributions: Ginga Shimakawa and Anja Krieger-Liszkay conceived the study, Ginga Shimakawa and Thomas Roach performed the experiments, Ginga Shimakawa prepared the data, Thomas Roach made the Figures, Thomas Roach and Anja Krieger-Liszkay wrote the manuscript, all authors proof-read the final submission.

Acknowledgements: The authors thank Dr Karin Krupinska (University of Kiel, Germany) for providing the barley seeds, Dr Wolfgang Stöggl and Dr Erwann Arc (University of Innsbruck) for analysis of RES and FAMEs. Ginga Shimakawa was supported by the LabEx Saclay Plant Sciences-SPS (grant number ANR-17-EUR-0007), the French Infrastructure for Integrated Structural Biology (FRISBI; grant number ANR-10-INSB-05) and the Japan Society for the Promotion of Science (grant number 16J03443). Thomas Roach and Anja Krieger-Liszkay thank the OeAD WTZ programme (FR

09/2018) and the Amadeus programme (PHC) for funding research exchange between Austria and France.

References

Bachmann A, Hause B, Maucher H, Garbe E, Vörös K, Weichert H, Wasternack C and Feussner I (2002) Jasmonate-induced lipid peroxidation in barley leaves initiated by distinct 13-LOX forms of chloroplasts. *Biological Chemistry* **383**:1645-1657.

Baker NR (2008) Chlorophyll fluorescence: a probe of photosynthesis in vivo. *Annual Review of Plant Biology* **59**:89-113.

Balazadeh S, Kwasniewski M, Caldana C, Mehrnia M, Zanor MI, Xue G-P and Mueller-Roeber B (2011) ORS1, an H2O2-responsive NAC transcription factor, controls senescence in *Arabidopsis thaliana*. *Molecular Plant* **4**:346-360.

Bieker S, Riester L, Stahl M, Franzaring J and Zentgraf U (2012) Senescence-specific Alteration of Hydrogen Peroxide Levels in *Arabidopsis thaliana* and Oilseed Rape Spring Variety *Brassica napus* L. cv. MozartF. *Journal of Integrative Plant Biology* **54**:540-554.

Biswas MS, Mano J (2021) Lipid Peroxide-Derived Reactive Carbonyl Species as Mediators of Oxidative Stress and Signaling. *Frontiers in Plant Science* **12**:720867.

Distelfeld A, Avni R and Fischer AM (2014) Senescence, nutrient remobilization, and yield in wheat and barley. *Journal of Experimental Botany* **65**:3783-3798.

Dogra V and Kim C (2020) Singlet Oxygen Metabolism: From Genesis to Signaling. *Frontiers in Plant Science* **10**:1640.

Farmer EE and Mueller MJ (2013) ROS-mediated lipid peroxidation and RES-activated signaling. *Annual Reviews in Plant Biology* **64**:429-450.

Garapati P, Xue G-P, Munné-Bosch S and Balazadeh S (2015) Transcription factor ATAF1 in Arabidopsis promotes senescence by direct regulation of key chloroplast maintenance and senescence transcriptional cascades. *Plant Physiology* **168**:1122-1139.

Gregersen PL, Holm PB and Krupinska K (2008) Leaf senescence and nutrient remobilisation in barley and wheat. *Plant Biology* **10**:37-49.

Griffiths G, Leverentz M, Silkowski H, Gill N and Sánchez-Serrano JJ (2000) Lipid hydroperoxide levels in plant tissues. *Journal of Experimental Botany* **51**:1363-1370.

Halliwell B (2006) Reactive species and antioxidants. Redox biology is a fundamental theme of aerobic life. *Plant Physiology* **141**:312-322.

Hu YR, Jiang YJ, Han X, Wang HP, Pan JJ and Yu DQ (2017) Jasmonate regulates leaf senescence and tolerance to cold stress: crosstalk with other phytohormones. *Journal of Experimental Botany* **68**:1361-1369.

Jajić I, Sarna T, Szewczyk G and Strzałka K (2015) Changes in production of reactive oxygen species in illuminated thylakoids isolated during development and senescence of barley. *Journal of Plant Physiology* **184**:49-56.

Klughammer C and Schreiber U (1994) An improved method, using saturating light pulses, for the determination of photosystem I quantum yield via $P700^{+}$-absorbance changes at 830 nm. *Planta* **192**:261–268.

Krieger-Liszkay A (2005) Singlet oxygen production in photosynthesis. *Journal of Experimental Botany* **56**:337-346.

Krieger-Liszkay A, Krupinska K and Shimakawa G (2019) The impact of photosynthesis on initiation of leaf senescence. *Physiologia Plantarum* **166**:148-164.

Krieger-Liszkay A and Trebst A (2006) Tocopherol is the scavenger of singlet oxygen produced by the triplet states of chlorophyll in the PSII reaction centre. *Journal of Experimental Botany* **57**:1677-1684.

Krieger-Liszkay A, Trösch M and Krupinska K (2015) Generation of reactive oxygen species in thylakoids from senescing flag leaves of the barley varieties Lomerit and Carina. *Planta* **241**:1497-1508.

Kumar A, Prasad A, Sedlářová M, Ksas B, Havaux M and Pospíšil P. (2020) Interplay between antioxidants in response to photooxidative stress in Arabidopsis. *Free Radicals in Biology and Medicine* **160**:894–907.

Lim PO, Kim HJ and Nam HG (2007) Leaf Senescence. *Annual Review of Plant Biology* **58**:115-136.

Lu C, Lu Q, Zhang J and Kuang T (2001) Characterization of photosynthetic pigment composition, photosystem II photochemistry and thermal energy dissipation during leaf senescence of wheat plants grown in the field. *Journal of Experimental Botany* **52**:1805-1810.

Mano J, Biswas MS and Sugimoto K (2019) Reactive Carbonyl Species: A Missing Link in ROS Signaling. *Plants* **8**:391.

Mano Ji (2012) Reactive carbonyl species: their production from lipid peroxides, action in environmental stress, and the detoxification mechanism. *Plant Physiology and Biochemistry* **59**:90-97.

Montillet JL, Cacas JL, Garnier L, Montané MH, Douki T, Bessoule JJ, Polkowska-Kowalczyk L, Maciejewska U, Agnel JP, Vial A and Triantaphylidès C (2004) The upstream oxylipin profile of *Arabidopsis thaliana*: a tool to scan for oxidative stresses. *The Plant Journal* **40**:439-451.

Nurbekova Z, Srivastava S, Standing D, Kurmanbayeva A, Bekturova A, Soltabayeva A, Oshanova D, Tureckova V, Strand M, Biswas MS, Mano J and Sagi M (2021) Arabidopsis aldehyde oxidase 3, known to oxidize abscisic aldehyde to abscisic acid, protects leaves from aldehyde toxicity. *The Plant Journal* **108**:1439-1455.

Pintó-Marijuan M and Munné-Bosch S (2014) Photo-oxidative stress markers as a measure of abiotic stress-induced leaf senescence: advantages and limitations. *Journal of Experimental Botany* **65**:3845-3857.

Ramel F, Mialoundama A and Havaux M (2013) Nonenzymic carotenoid oxidation and photoxidative stress signalling plants. *Journal of Experimental Botany* **64**:799-805.

Roach T, Baur T, Stoggl W and Krieger-Liszkay A (2017) *Chlamydomonas reinhardtii* responding to high light: a role for 2-propenal (acrolein). *Physiologia Plantarum* **161**:75-87.

Roach T and Krieger-Liszkay A (2019) Photosynthetic Regulatory Mechanisms for Efficiency and Prevention of Photo-Oxidative Stress, in *Annual Plant Reviews online*. **2**:1.

Roach T, Na CS, Stöggl W and Krieger-Liszkay A (2020) The non-photochemical quenching protein LHCSR3 prevents oxygen-dependent photoinhibition in *Chlamydomonas reinhardtii*. *Journal of Experimental Botany*. **71**:2650–2660.

Roach T, Stoggl W, Baur T and Kranner I (2018) Distress and eustress of reactive electrophiles and relevance to light stress acclimation via stimulation of thiol/disulphide-based redox defences. *Free Radicals in Biology and Medicine* **122**:65-73.

Schausberger C, Roach T, Stoggl W, Arc E, Finch-Savage WE and Kranner I (2019) Abscisic acid-determined seed vigour differences do not influence redox regulation during ageing. *Biochemical Journal* **476**:965-974.

Schneider C, Boeglin WE, Yin H, Stec DF, Hachey DL, Porter NA and Brash AR (2005) Synthesis of dihydroperoxides of linoleic and linolenic acids and studies on their transformation to 4-hydroperoxynonenal. *Lipids* **40**:1155-1162.

Seltmann MA, Stingl NE, Lautenschlaeger JK, Krischke M, Mueller MJ and Berger S (2010) Differential impact of lipoxygenase 2 and jasmonates on natural and stress-induced senescence in Arabidopsis. *Plant Physiology* **152**:1940-1950.

Shimakawa G, Roach T and Krieger-Liszkay A (2020) Changes in Photosynthetic Electron Transport during Leaf Senescence in Two Barley Varieties Grown in Contrasting Growth Regimes. *Plant and Cell Physiology* **61**:1986-1994.

Shimakawa G, Suzuki M, Yamamoto E, Saito R, Iwamoto T, Nishi A and Miyake C (2014) Why don't plants have diabetes? Systems for scavenging reactive carbonyls in photosynthetic organisms. *Biochemical Society transactions* **42**:543-547.

Springer A, Kang C, Rustgi S, von Wettstein D, Reinbothe C, Pollmann S and Reinbothe S (2016) Programmed chloroplast destruction during leaf senescence involves 13-lipoxygenase (13-LOX). *Proceedings of the National Academy of Sciences, USA* **113**:3383-3388.

Srivastava S, Brychkova G, Yarmolinsky D, Soltabayeva A, Samani T and Sagi M (2017) Aldehyde Oxidase 4 Plays a Critical Role in Delaying Silique Senescence by Catalyzing Aldehyde Detoxification. *Plant Physiology* **173**:1977-1997.

Sunkar R, Bartels D and Kirch H-H (2003) Overexpression of a stress-inducible aldehyde dehydrogenase gene from *Arabidopsis thaliana* in transgenic plants improves stress tolerance. *The Plant Journal* **35**:452-464.

Thomas H (2013) Senescence, ageing and death of the whole plant. *New Phytol* **197**:696-711.

Triantaphylidès C, Krischke M, Hoeberichts FA, Ksas B, Gresser G, Havaux M, Van Breusegem F and Mueller MJ (2008) Singlet oxygen is the major reactive oxygen species involved in photooxidative damage to plants. *Plant Physiology* **148**:960-968.

van Wijk KJ, Kessler F (2017) Plastoglobuli: Plastid Microcompartments with Integrated Functions in Metabolism, Plastid Developmental Transitions, and Environmental Adaptation. *Annual Review of Plant Biology* **68**:253-289

Wewer V, Dörmann P and Hölzl G (2013) Analysis and Quantification of Plant Membrane Lipids by Thin-Layer Chromatography and Gas Chromatography. In Munnik, T. & Heilmann, I. (Eds.) Plant Lipid Signaling Protocols, Totowa: Humana Press, pp. 69-78.

Zentgraf U, Andrade-Galan AG and Bieker S (2022) Specificity of H_2O_2 signaling in leaf senescence: is the ratio of H2O2 contents in different cellular compartments sensed in Arabidopsis plants? *Cellular & Molecular Biology Letters* **27**:4.

Zentgraf U and Doll J (2019) Arabidopsis WRKY53, a Node of Multi-Layer Regulation in the Network of Senescence. *Plants* **8**:578.

Figure legends:

Figure 1. Changes in photosynthesis-related parameters during sequential senescence in barley leaves of cv. Lomerit (closed symbols) and cv. Carina (open symbols). (A) Maximum quantum yields of photosystem II (F_v/F_m; circles) and maximum redox change of photosystem I (P_m; squares) of first-emerging leaves after 13, 20 and 27 days (first time course) or 18, 25 and 32 days (second time course) after sowing seeds, with all changes shown relative to values of pre-senescent leaves (13 days), means ±SD, n=6 for each genotype at each time point. (B, C) Relationship of P_m values with (B) F_v/F_m , and (C) total chlorophyll (a+b) concentrations, with each data point representing an individual leaf.

Figure 2. Relationship between maximum redox change of photosystem I (P_m), used as a senescence marker, and xanthophyll cycle de-epoxidation ratios (VAZ de-epox.), and changes in non-photochemical quenching (NPQ), during sequential senescence of first-emerging barley leaves of cv. Lomerit (closed symbols) and cv. Carina (open symbols). (A) Each data point represents an individual leaf, V: Violaxanthin; A: antheraxanthin; Z zeaxanthin. (B) NPQ values of leaves after 13, 20 and 27 days after sowing seeds, means of each time point ±SD, with different letters denoting significant differences at P<0.05, n=6 leaves for each genotype at each time point.

Figure 3. Concentrations of aldehydes and RES, as markers of lipid peroxidation, during sequential senescence of first-emerging barley leaves. Differences for cv. Carina (C) and cv. Lomerit (L), and for each time after sowing seeds (indicated left), are shown relative to pre-senescent leaves (average of both cultivars 13 days after sowing seeds), as $\log_2$ values on a colour scale (shown below). Data has been normalised to (A) total chlorophyll, and (B) measured leaf area, with * and ** denoting significant differences at P<0.05 and P<0.01, respectively, n=6 leaves for each cultivar at each time point. (C) Leaf lipoxygenase activity in cv. Carina relative to maximum redox change of photosystem I (P_m), used as a senescence marker.

Figure 4. Relationship between maximum redox change of photosystem I (P_m), used as a senescence marker, and tocopherol concentrations during sequential senescence in first-emerging barley leaves. (A) α-tocopherol (circles) and γ-tocopherol (squares) normalised to total chlorophyll in leaves of cv. Lomerit (closed symbols) and cv. Carina (open symbols). Each data point represents an individual leaf with all data shown from both time courses. (B) Concentrations of α-tocopherol normalised to leaf area in cv. Carina and cv. Lomerit.

Figure 5. Changes in fatty acids (FA) and membrane lipids during sequential senescence in first-emerging barley leaves of cv. Carina. (A) Percentage of each FA in total leaf FAs, in pre-senescent leaves 18 days (d) after sowing seeds. Species are denoted by acyl chain length followed by number of double bonds; linolenic acid (C18:3), palmitic acid (C16:0), linoleic acid (C18:2), stearic acid (C18:0),

and palmitoleic acid (C16:1). (B) Fold difference of each fatty acid between 18 d and 25 d (blue), and 25 d and 32 d (yellow) on a $\log_2$ scale. Asterisks denote a significant change compared to the previous time period (P<0.05). (C) Relative difference of membrane lipids between 18 d and 32 d (n = 4), as quantified by band intensity after separation of total lipid extracts by thin layer chromatography, as shown in (D). All data are normalised to leaf DW.

Figure 6. A bi-plot principal component analysis (PCA) of photosynthetic and lipid peroxide-related parameters during developmental senescence of first-emerging barley leaves. Each data point, separated in PC1 (bottom x axis) and PC2 (left y axis), represents an individual mid-leaf segment of cv. Lomerit (L) and cv. Carina (C), coloured by age, into groups 1 (13 days since sowing; purple), 2 (18 or 20 days since sowing; red), 3 (25 or 27 days since sowing; yellow) or 4 (32 days since sowing; green). Overlaid is the loading plot (right y and top x axes), showing established senescence indicators (black, dotted line), photosynthetic pigments and tocopherols (blue), and all detected lipid peroxide breakdown products (grey).

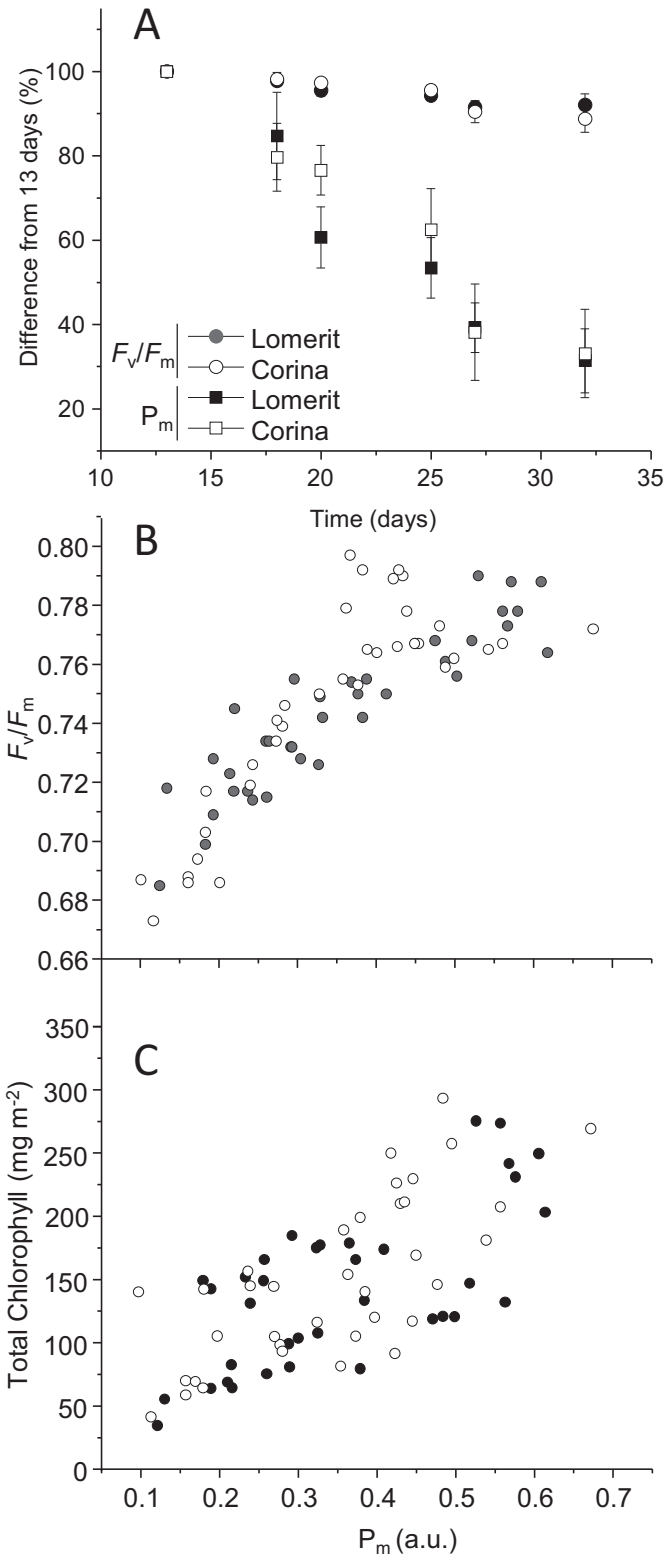
A
Difference from 13 days (%)
100
80
60
40
20
10
15
20
25
30
35
Time (days)
F_v/F_m
Lomerit
Corina
P_m
Lomerit
Corina
B
F_v/F_m
0.80
0.78
0.76
0.74
0.72
0.70
0.68
0.66
C
Total Chlorophyll (mg m^{-2})
350
300
250
200
150
100
50
0
0.1
0.2
0.3
0.4
0.5
0.6
0.7
P_m (a.u.)

Figure 1

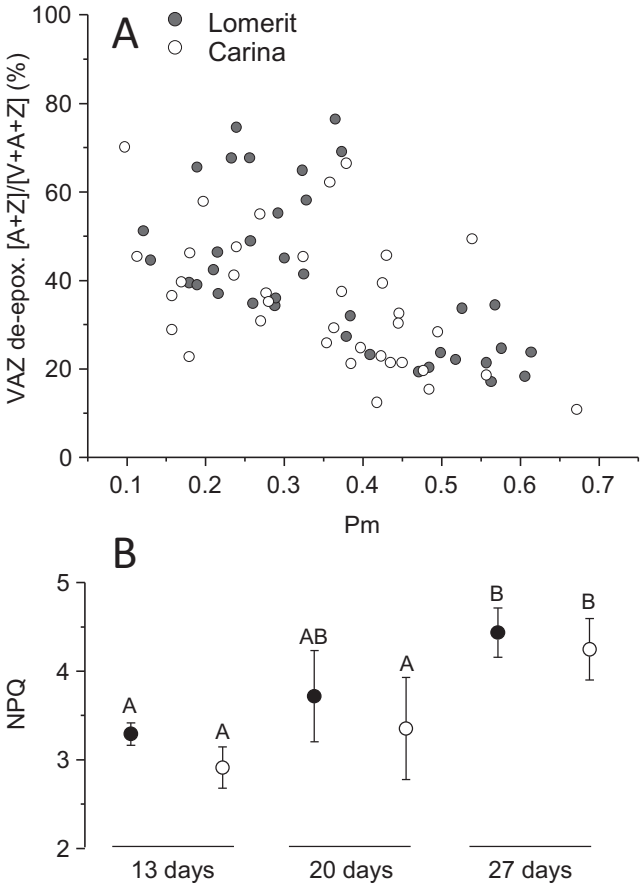
A
Lomerit
Carina
VAZ de-epox. [A+Z]/[V+A+Z] (%)
100
80
60
40
20
0
0.1
0.2
0.3
0.4
0.5
0.6
0.7
Pm
B
NPQ
5
4
3
2
A
A
AB
A
B
B
13 days
20 days
27 days

Figure 2

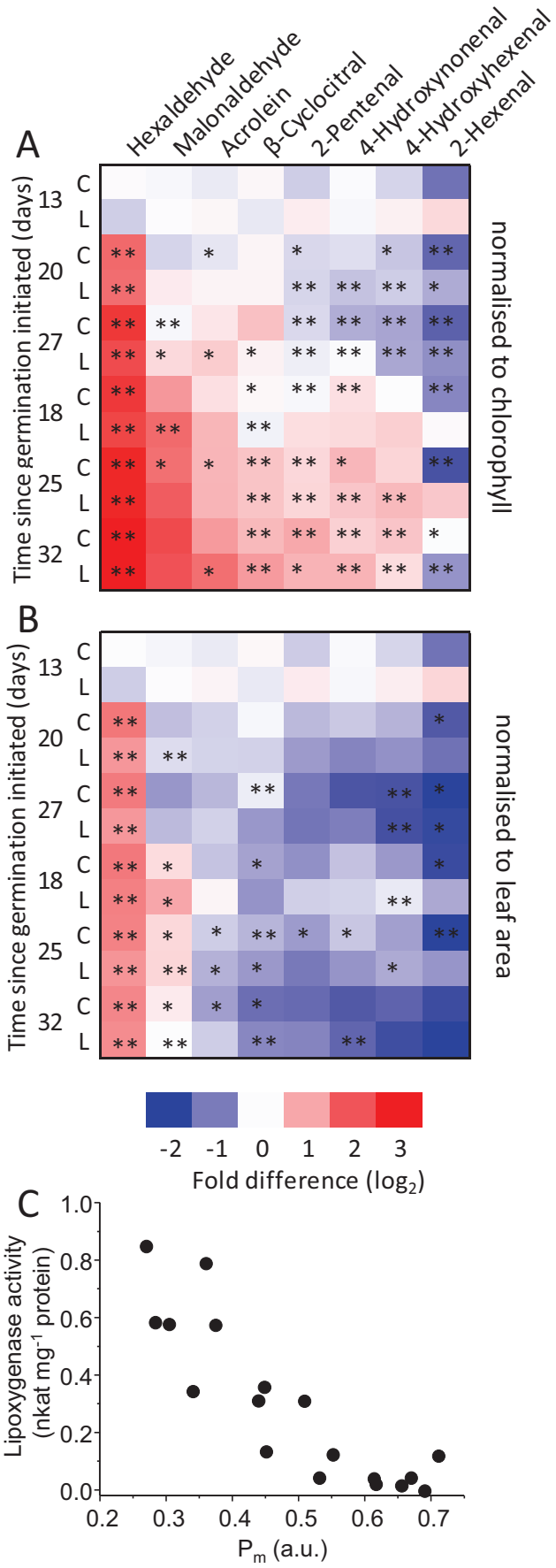
A
B
C
Hexaldehyde
Malonaldehyde
Acrolein
β-Cyclocitral
2-Pentenal
4-Hydroxynonenal
4-Hydroxyhexenal
2-Hexenal
Time since germination initiated (days)
13
20
27
18
25
32
C
L
normalised to chlorophyll
normalised to leaf area
-2 -1 0 1 2 3
Fold difference (log2)
Lipoxygenase activity (nkat mg-1 protein)
1.0
0.8
0.6
0.4
0.2
0.0
0.2 0.3 0.4 0.5 0.6 0.7
Pm (a.u.)

Figure 3

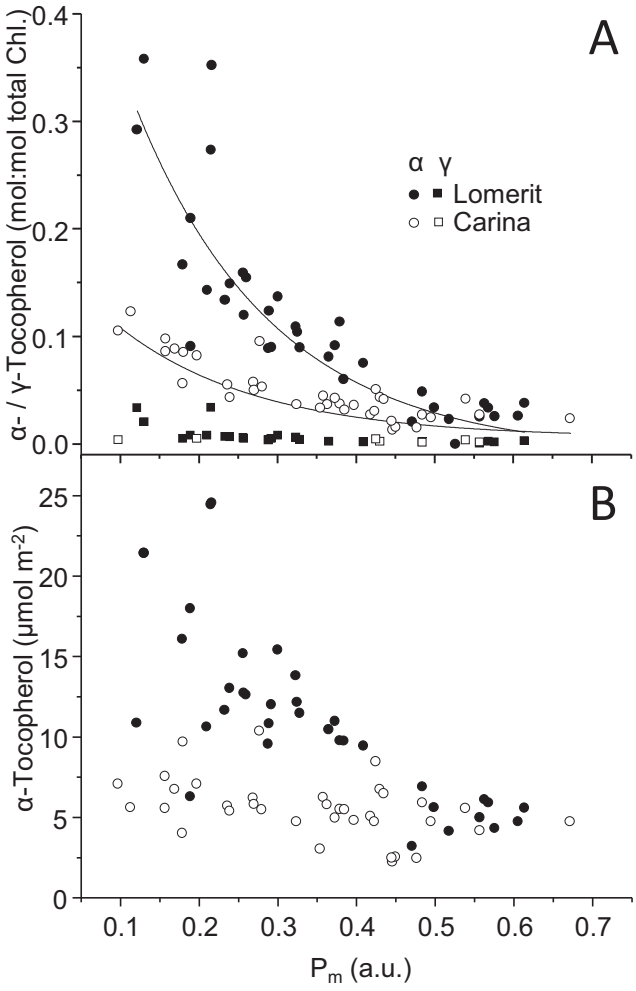
A
B
α- / γ-Tocopherol (mol:mol total Chl.)
α γ
Lomerit
Carina
α-Tocopherol (µmol m-2)
Pm (a.u.)
0.0
0.1
0.2
0.3
0.4
0
5
10
15
20
25
0.1
0.2
0.3
0.4
0.5
0.6
0.7

Figure 4

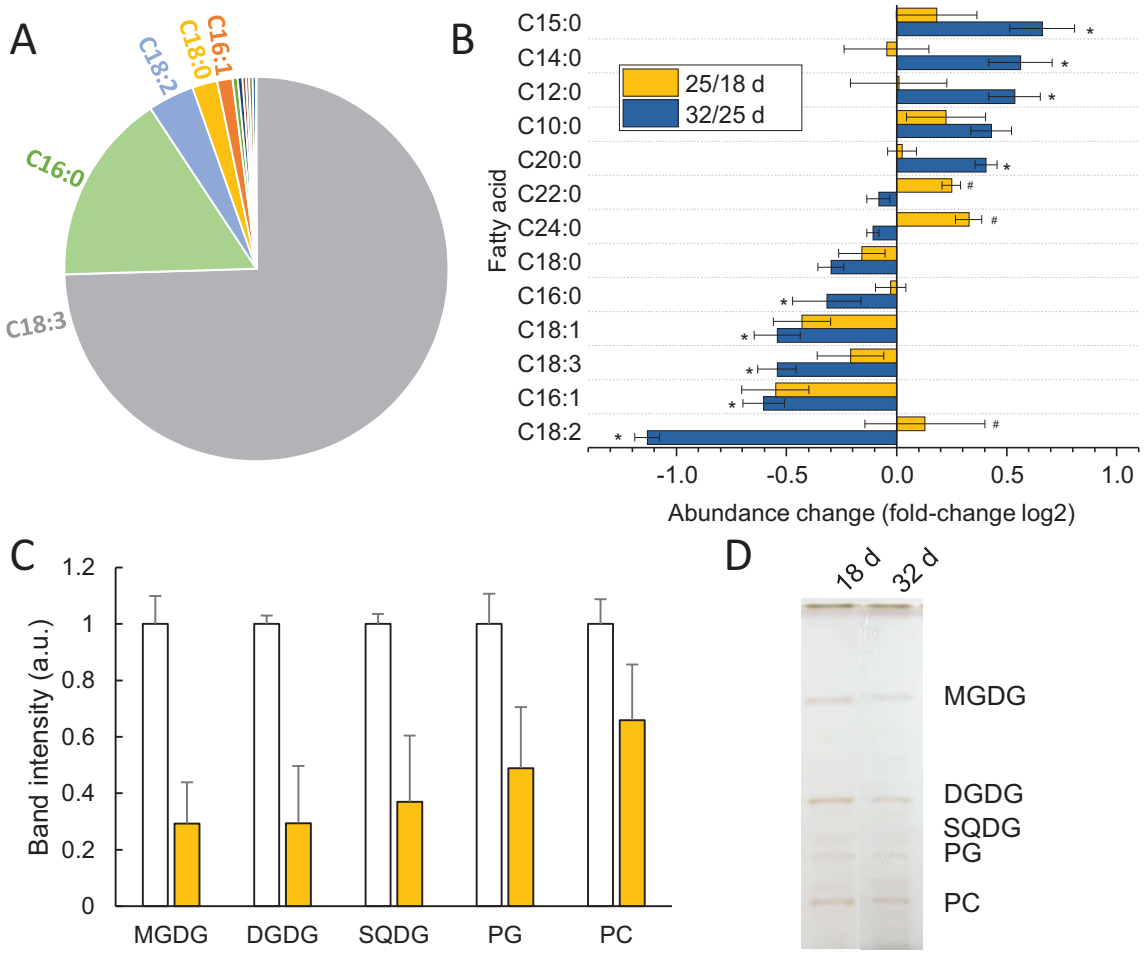
A
C16:1
C18:0
C18:2
C16:0
C18:3
B
C15:0
C14:0
C12:0
C10:0
C20:0
C22:0
C24:0
C18:0
C16:0
C18:1
C18:3
C16:1
C18:2
25/18 d
32/25 d
Fatty acid
-1.0
-0.5
0.0
0.5
1.0
Abundance change (fold-change log2)
C
Band intensity (a.u.)
1.2
1
0.8
0.6
0.4
0.2
0
MGDG
DGDG
SQDG
PG
PC
D
18 d
32 d
MGDG
DGDG
SQDG
PG
PC

Figure 5

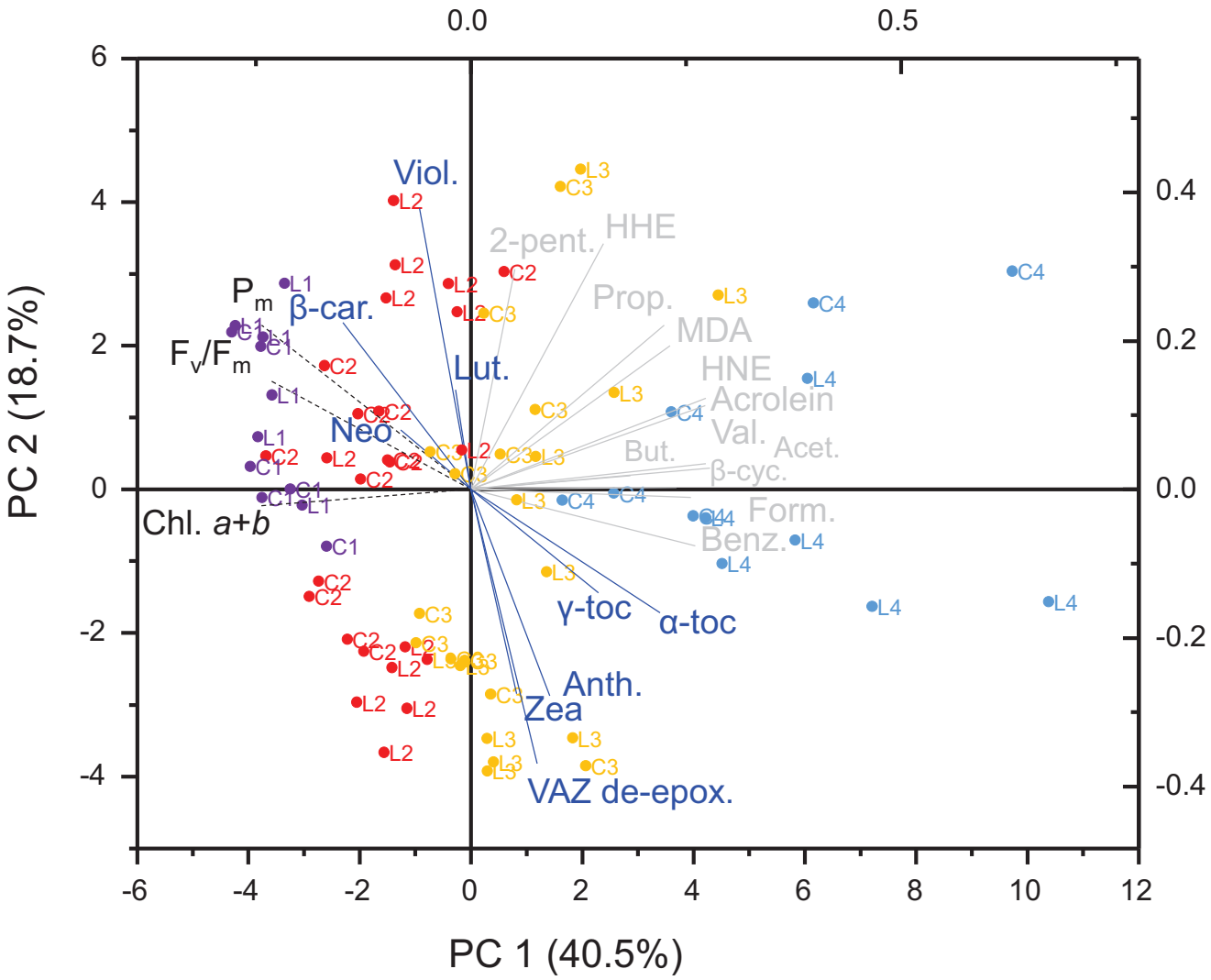
0.0
0.5
6
4
2
0
-2
-4
0.4
0.2
0.0
-0.2
-0.4
-6
-4
-2
0
2
4
6
8
10
12
PC 2 (18.7%)
PC 1 (40.5%)
Viol.
2-pent.
HHE
Prop.
MDA
HNE
Acrolein
Val.
Acet.
But.
β-cyc.
Form.
Benz.
Lut.
Neo
Chl. a+b
γ-toc
α-toc
Anth.
Zea
VAZ de-epox.
P m
β-car.
F v/F m

Figure 6

Supplemental Table 1. Statistical analysis using a univariate general linear model to calculate *P* values between the cultivars and over time, including data from both time courses (n = six replicates each for the six time points). Significant values where $P<0.05$ are labelled red.

	P values			
	Cultivar	Time	Cultivar	Time
F_v/F_m	0,699	<0.001		
P_m	0,479	<0.001		
	Normalised to chlorophyll		Normalised to leaf area	
Total Chlorophyll			0,238	<0.001
Chl a:b			0,862	0,332
Acrolein	0,007	<0.001	0,001	<0.001
Propionaldehyde	0,506	<0.001	0,475	<0.001
Malondialdehyde	0,634	<0.001	0,084	<0.001
trans-2-hex	0,011	<0.001	0,006	<0.001
trans-2-pent	0,176	0,061	0,111	<0.001
β-cyclocitral	0,956	<0.001	0,007	<0.001
4-HHE	0,545	0,072	0,155	<0.001
4-HNE	0,989	<0.001	0,68	<0.001
Formaldehyde	0,118	<0.001	0,95	0,002
Acetylaldehyde	0,056	<0.001	0,369	0,005
Hexaldehyde	0,56	<0.001	0,003	<0.001
Butyraldehyde	<0.001	<0.001	<0.001	<0.001
Benzylaldehyde	0,953	<0.001	0,078	<0.001
Valeraldehyde	0,001	<0.001	<0.001	0,001
Neoxanthin	0,065	0,133		
Violaxanthin	0,222	0,002		
Antheraxanthin	<0.001	0,082		
Lutein	0,145	0,812		
Zeaxanthin	0,024	0,129		
β-carotene	0,113	<0.001		
α-tocopherol	<0.001	<0.001		
VAZ DEP (A+Z)/(V+A+Z)	0,169	<0.001		

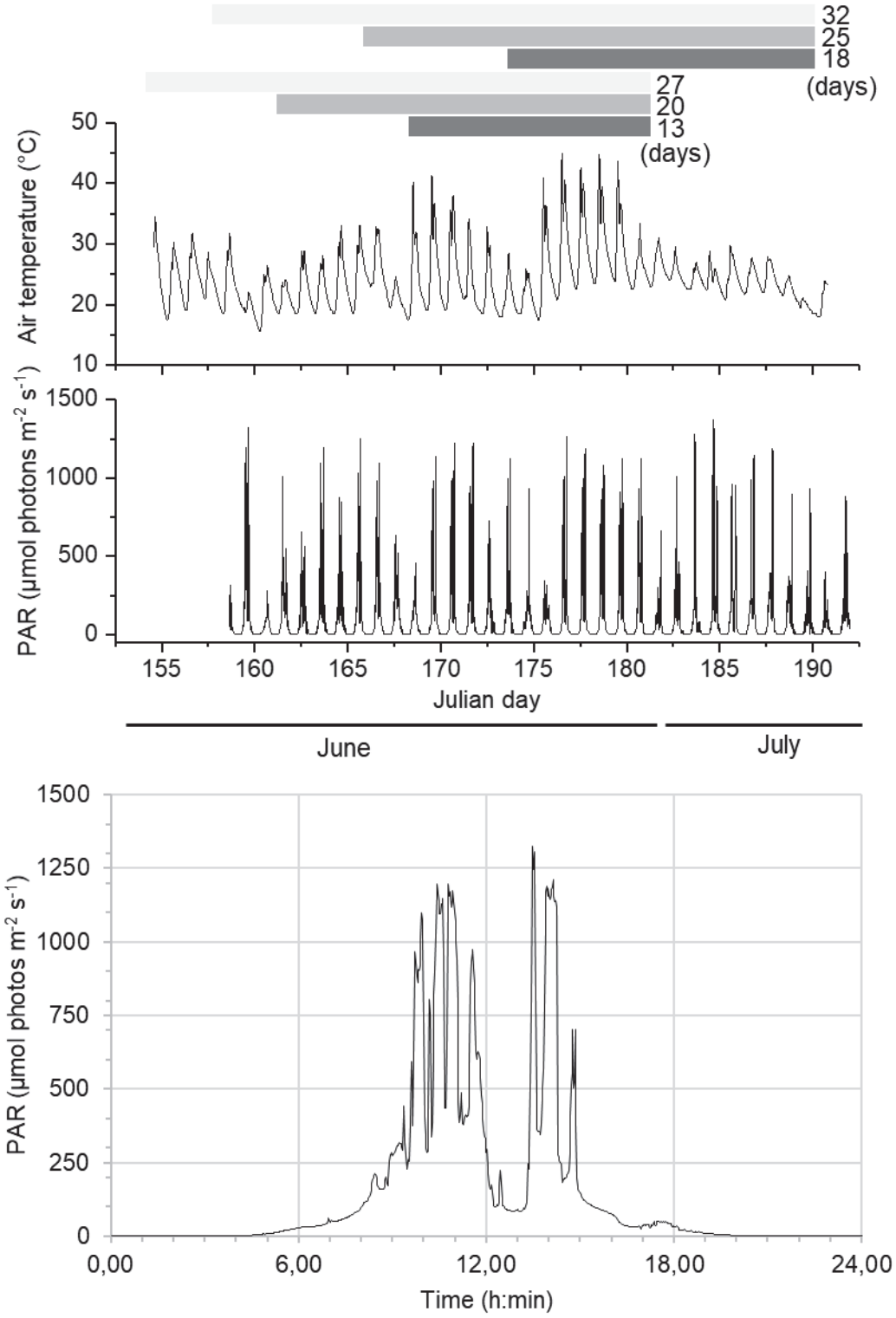

Supplementary Figure 1. Climatic conditions in the glass house used for growing the barley plants. (A) The grey bars above indicate when plants were grown, starting with the day when seeds were sown and ending when measurements were made. (B) Typical light intensity on a cloudless day. PAR: Photoysnthetic active radiation

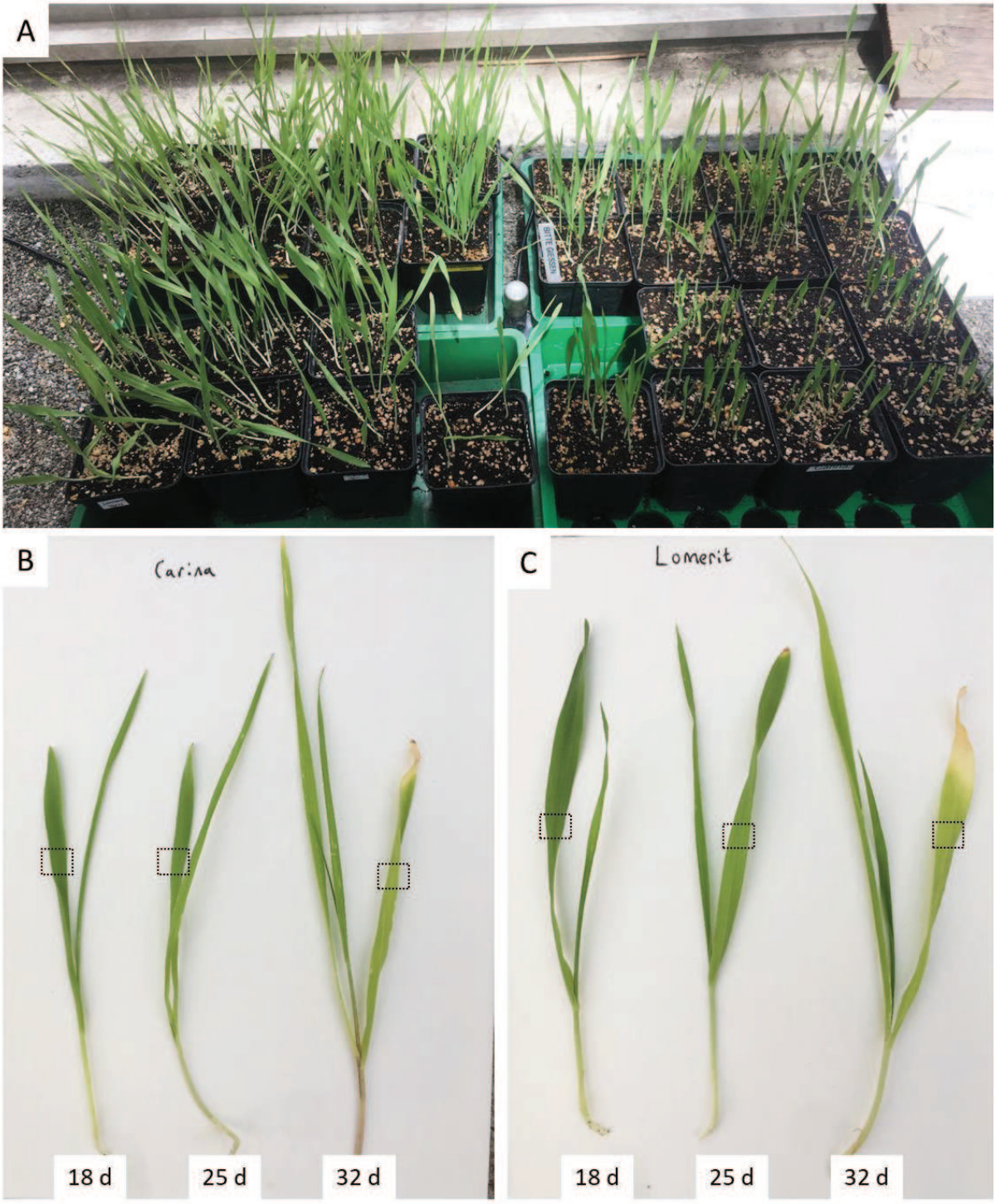

Supplementary Figure 2. Image of the barely plants of different ages used for experiments, here just after watering. Typical plants after 18, 25 and 32 days (d) since sowing of (B) cv. Carina and (C) cv. Lomerit. The black dashed boxes indicate the midpoint of primary leaves measured.

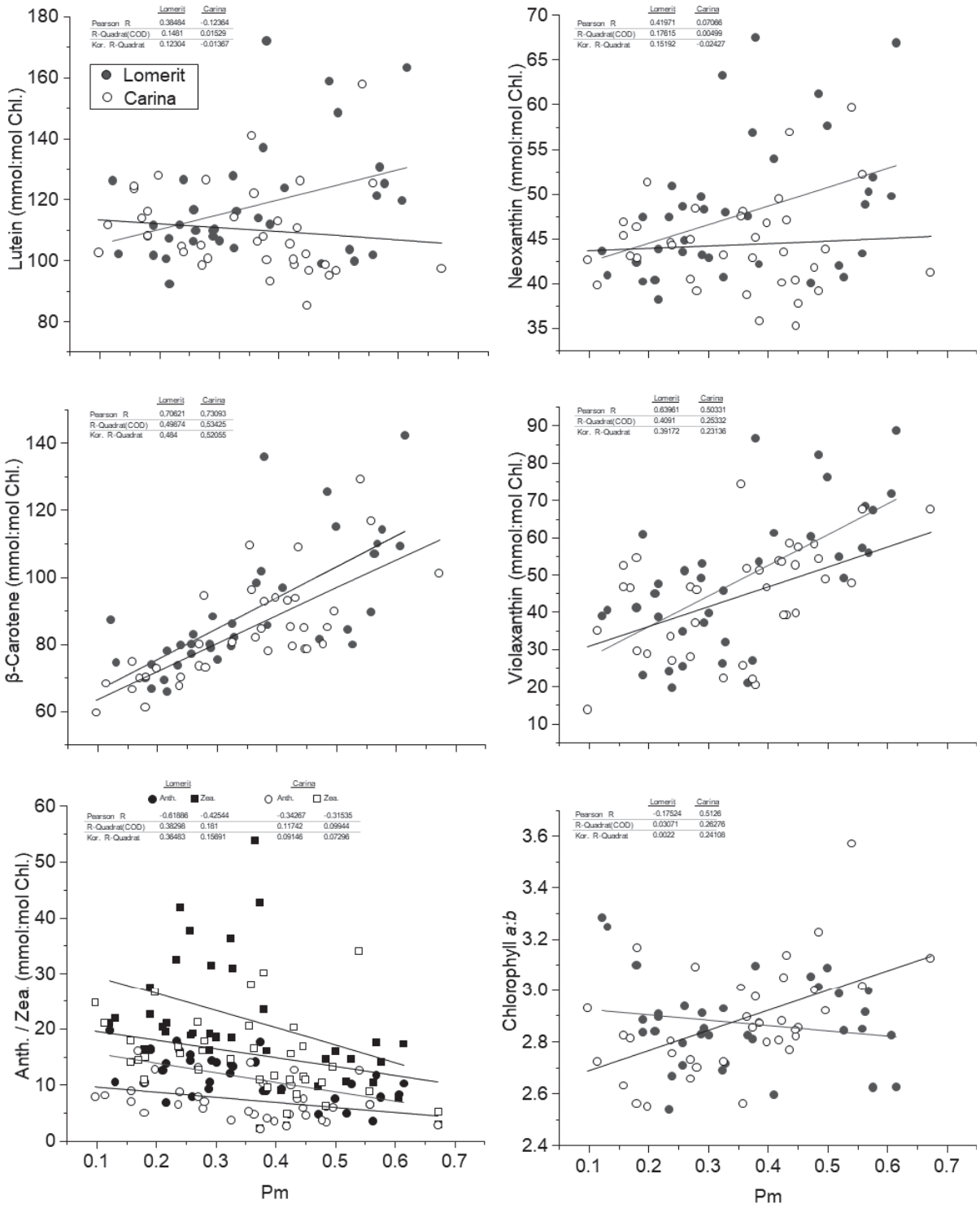

Supplementary Figure 3. Concentrations of carotenoids, normalised to total chlorophyll content (Chl.), and chlorophyll *a*:*b* ratio, relative to changes in maximum photo-oxidizable P700 levels (P_m) in primary leaves of barley cultivars Lomerit and Carina.

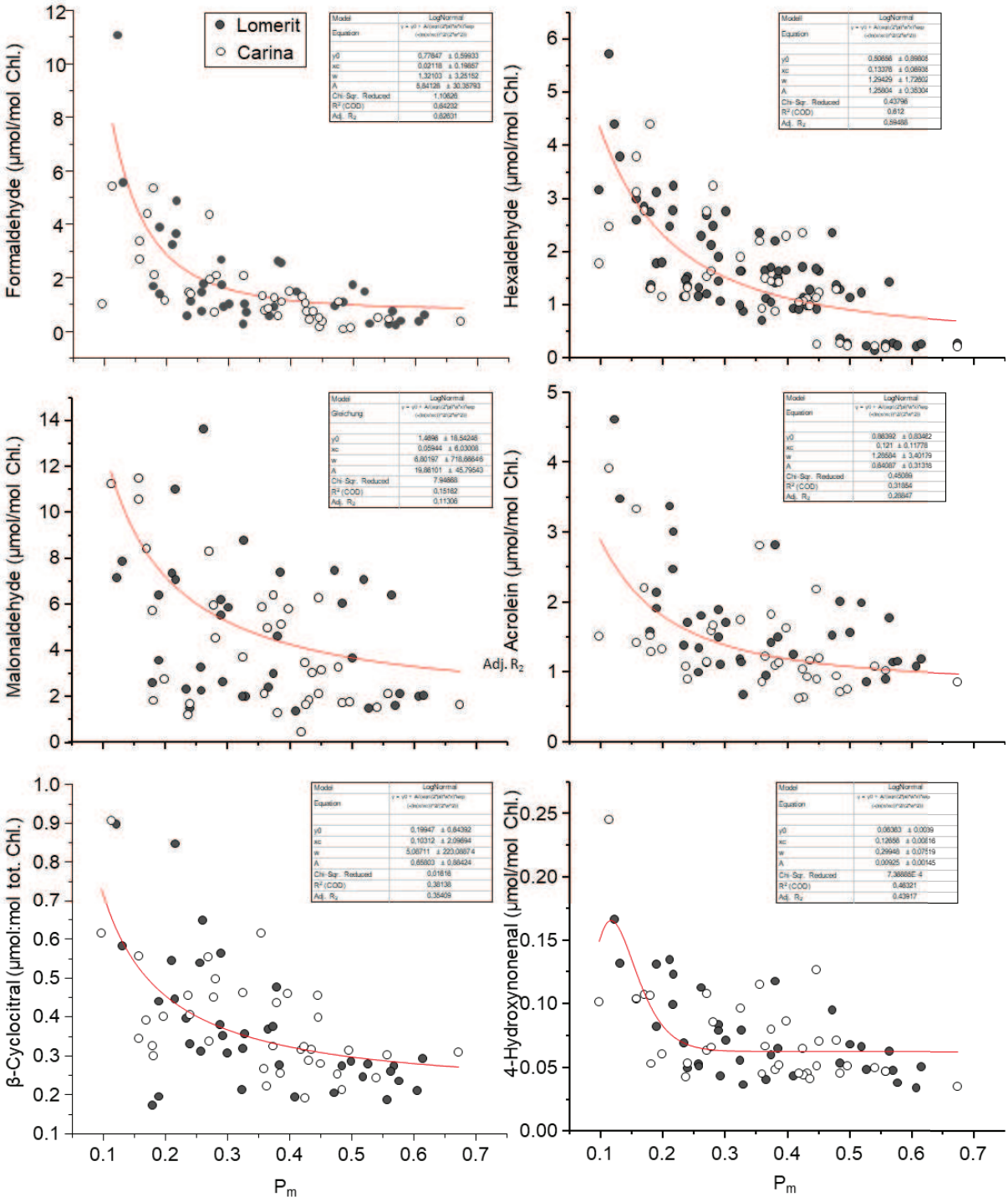

Supplementary Figure 4. Absolute concentrations of aldehyde, including reactive electrophile species (malonaldehyde, acrolein, β-cyclocitral and 4-Hydroxynonenal), normalised to total chlorophyll content (Chl.), relative to changes in maximum photo-oxidizable P700 levels (P_m) in primary leaves of barley cultivars Lomerit and Carina.